

Experiments with the nonlinear and chaotic behaviour of the multiplicative algebraic reconstruction technique (MART) algorithm for computed tomography

Cristian Badea¹ and Richard Gordon²

¹ Center for In Vivo Microscopy, Box 3302 Duke Medical Center, Durham, NC 27710, USA

² Department of Radiology and TRILabs, University of Manitoba, Health Sciences Centre, 820 Sherbrook Street, Winnipeg, MB R3A 1R9 Canada

E-mail: chris@orion.duhs.duke.edu and GordonR@ms.UManitoba.ca

Received 10 September 2003, in final form 16 February 2004

Published 24 March 2004

Online at stacks.iop.org/PMB/49/1455 (DOI: 10.1088/0031-9155/49/8/006)

Abstract

Among the iterative reconstruction algorithms for tomography, the multiplicative algebraic reconstruction technique (MART) has two advantages that make it stand out from other algorithms: it confines the image (and therefore the projection data) to the convex hull of the patient, and it maximizes entropy. In this paper, we have undertaken a series of experiments to determine the importance of MART nonlinearity to image quality. Variants of MART were implemented aiming to exploit and exaggerate the nonlinear properties of the algorithm. We introduce the Power MART, Boxcar Averaging MART and Bouncing MART algorithms. Power MART is linked to the relaxation concept. Its behaviour is similar to that of the chaos of a logistic equation. There appears to be an antagonism between increasing nonlinearity and noise in the projection data. The experiments confirm our general observation that regularization as a means of solving simultaneous linear equations that are underdetermined is suboptimal: it does not necessarily select the correct image from the hyperplane of solutions, and so does not maximize the image quality:x-ray dose ratio. Our investigations prove that there is scope to optimize CT algorithms and thereby achieve greater dose reduction.

1. Introduction

MART (multiplicative algebraic reconstruction technique) is a nonlinear iterative algorithm for CT (computed tomography) image reconstruction (Gordon *et al* 1970) with the desirable properties that: (a) it converges to and selects for the one solution of the simultaneous, usually underdetermined set of linear CT equations that maximizes entropy (Lent 1977,

Lent and Censor 1991, Darroch and Ratcliff 1972); and (b) it confines the reconstruction to the convex hull of the object (Meisters and Ulam 1967, Beyer and Ulam 1968, Chaudhuri and Rosenfeld 1998). With the revival of iterative algorithms for CT, in the context of cone beam reconstruction for multislice CT (Donaire and Garcia 1999, Mueller *et al* 1999a, 1999b, Mueller *et al* 2000, Mueller and Yagel 2000, Wang *et al* 1999, Badea 2000, Hsieh *et al* 2000, Chlewicki 2001), and the high total patient doses that are now occurring, with CT representing 40–75% of the population dose (Kalender 2000, Crawley *et al* 2001, Wiest *et al* 2002), it is time to readdress the issue of dose reduction in CT (Gordon 1976). From Wiest *et al* (2002) we may estimate that at present the ratio of the dose of an average CT to the dose of an average non-CT x-ray examination is 16. The total dose per person to the population, including CT, is now at a level four times that before CT, and is on the increase.

We think that dose reduction may be possible, that goes well beyond alternate beam filtering (Itoh *et al* 2001), digital filtering (Kachelriess *et al* 2001), tailoring technique to patient size (Donnelly *et al* 2001, Paterson *et al* 2001, Kalra *et al* 2002) or beam modulation according to cross-sectional shape of the patient (Kalender *et al* 1999, Greess *et al* 1999, 2000, 2001, 2002, Mastora *et al* 2001, Lehmann *et al* 1997, Giacomuzzi *et al* 1996), by *revamping the CT algorithms themselves*. Towards this goal, we have undertaken a series of experiments to determine the importance of the degree of MART nonlinearity for image quality. Variants of MART were devised and implemented aiming to exploit and exaggerate the nonlinear properties of the algorithm. To our surprise, we reached a threshold at which MART became chaotic in its behaviour.

The convex hull property of the MART algorithm is clinically important: it automatically approximates the convex hull of the patient, and thus most of the data are driven into the region occupied by the patient, resulting in an increased image quality:dose ratio. The *convex hull* is defined as the envelope of all straight lines that touch an object at its perimeter or surface, but do not cross the object (Meisters and Ulam 1967, Beyer and Ulam 1968, Chaudhuri and Rosenfeld 1998). For the two-dimensional case, we define the *CT convex hull* as a polygon designated by the intersection of two sets: (a) the rays used in acquiring a set of CT data and (b) the straight lines defining the convex hull. MART confines the reconstruction to the CT convex hull of the object, which is, in general, just marginally larger than the convex hull. This is a modest improvement over additive ART, which confines the data to a square around the patient, and a vast improvement over the industry-standard filtered backprojection (see FBP for cone beam CT: Cho *et al* 1994, Defrise and Clack 1994, Weng *et al* 1996, Kudo *et al* 1998, 2000, Kudo and Saito 1998, Tang and Ning 2001, Tam *et al* 2002), which scatters image over infinite space. Thus, as the CT community turns to 3D iterative algorithms, we suggest that the best choices will be MART-like algorithms.

2. Methods

The original MART algorithm (Gordon *et al* 1970) can be written as

$$x_j^{k+1} = x_j^k \left(\frac{y_i}{H_{ik}x^k} \right)^{\gamma h_{ij}} \quad (1)$$

where x_j^k and x_j^{k+1} are the successive estimates at iterations k and $k + 1$ of the reconstructed value for the j th ray; y_i and $H_{ik}x^k$ are the projection and the reprojection values corresponding to the i th ray; H is the projection operator applied on the current x^k image; γ is the relaxation factor and h_{ij} represents the contribution of reconstruction ray i and pixel j . Note that there is a different ray j generated for each distinct position of each detector array and/or the x-ray source, if a moving gantry is used.

2.1. Power MART and the relaxation concept

In expression (1), by notation, the correction error ratio is $c = y_i/H_{ik}x^k$. Thus, the multiplicative updating of ray j in the reconstructed image becomes, for $\gamma = 1$,

$$x^{k+1} = x^k c^p \quad (2)$$

where $p = 1$ for $h_{ij} = 1$ and $p = 0$ for $h_{ij} = 0$ (binary weighting: Gordon and Herman 1974). In our study, we have tested, when $h_{ij} = 0$ or 1 , $p = \{0.5, 1, 1.9, 2, 2.1\}$, and named the new algorithms (for $p \neq 1$) 'Power MART'. The motivation for doing this is that higher powers sharpen features along a ray that develop during the reconstruction process. Different power exponents applied to the correction factor were also used with the Expectation Maximization algorithm to alter the speed of convergence and to have a uniform correction efficiency at all spatial frequencies (Tanaka 1987).

Expression (2) is equivalent to

$$x^{k+1} = x^k (1 + c - 1)^p \quad (3)$$

and if we make the assumption that $c - 1 \ll 1$, i.e., that the normalized error $c - 1 = (y_i - H_{ik}x^k)/H_{ik}x^k \ll 1$, we can take the first term in the Taylor expansion of (3):

$$x^{k+1} = x^k (1 + p(c - 1)) \quad x^{k+1} = (1 - p)x^k + px^k c. \quad (4)$$

Expression (4) is the well-known RAMLA algorithm (Browne and De Pierro 1996). In Censor *et al* (1989), it was proved that MART is a particular case of Bregman's relaxed algorithm introduced in De Pierro and Iusem (1986), that is, for a given p there is a value of Bregman's relaxation parameter that gives rise to MART.

2.2. Critical power

According to our tests, Power MART using $p > 2$ power exponents leads to divergence of the reconstruction process and to the collapse of the image even for the well-determined case. Figure 1 presents the reconstructed images of a modified Shepp and Logan phantom available in MATLAB (The MathWorks, Natick, MA) version 6.5, with $n^2 = 157 \times 157$ pixels, $M = 128$ projections, using Power MART with different exponents $p = \{1, 1.9, 2, 2.1\}$. The detailed description of the phantom is given in table 1. Note that $p < 2$ involves convergence, $p = 2$ cycles between two false solutions shown here at the fifth (b) and tenth iterations (c), while $p = 2.1$ causes collapse of the image even before the first iteration. The power exponent leading to the collapse of the reconstructed image was named the *critical power*. The critical power is $p_c = 2$. Some understanding of the convergence/divergence of the Power MART algorithm is attained if we look at equation (2) as a recursive series with p as a parameter that determines the behaviour. Indeed, let us consider an image made of a single pixel and two projections (horizontal and vertical) and study Power MART for $p = \{0.5, 1.0, 2.0, 2.1\}$. Both the reconstructed value and the correction ratio after each cycle (or view) are shown in figures 2(a) and (b). It can be noticed that $p = 0.5$ involves more cycles until the reconstruction converges. In a fully convergent case, the correction ratio should converge and stabilize towards the value $c = 1$ corresponding to the situation where the projections and reprojections are matched. The divergence of the algorithm that finally produces the collapse of the reconstruction image can be recognized by the increasing amplitudes both in the correction ratio c and the reconstructed values.

Chaos is present if starting from two very close seeds (i.e., initial solutions) x_0 and $x_0 + \varepsilon$ we would obtain growing differences the more we iterate. The chaotic behaviour is shown in figure 2(c) where values of $p > 2$ clearly display growing amplitudes as the number of iterations

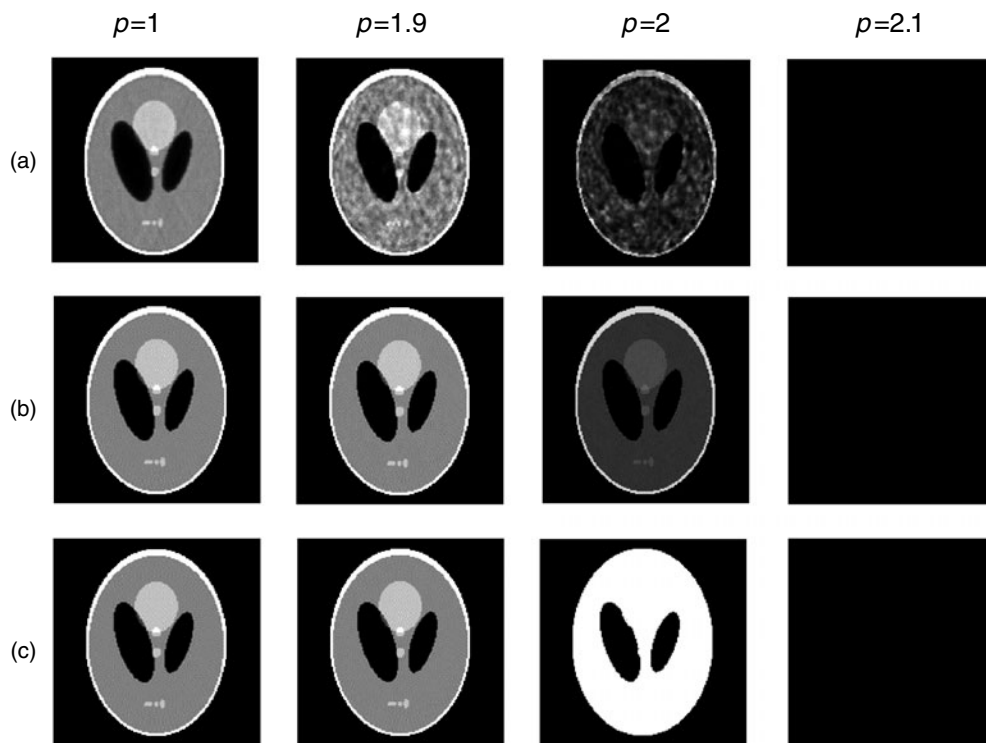


Figure 1. The Shepp and Logan phantom: Power MART reconstructions for $p = \{1, 1.9, 2, 2.1\}$ after first (a), fifth (b) and tenth (c) iterations. Note that $p < 2$ converges, $p = 2$ cycles between two false solutions shown here at iterations 5 (b) and 10 (c), while $p = 2.1$ causes the collapse of the image even before iteration 1.

Table 1. A modified Shepp and Logan head phantom.

Ellipse	Variables					
	A	a	B	x_0	y_0	ϕ
1	1	0.69	0.92	0	0	0
2	-0.8	0.6624	0.874	0	-0.0184	0
3	-0.2	0.11	0.31	0.22	0	-18
4	-0.2	0.16	0.41	-0.22	0	18
5	0.1	0.21	0.25	0	0.35	0
6	0.1	0.046	0.046	0	0.1	0
7	0.1	0.046	0.046	0	-0.1	0
8	0.1	0.046	0.023	-0.08	-0.605	0
9	0.1	0.023	0.023	0	-0.606	0
10	0.1	0.023	0.046	0.06	-0.605	0

A is the additive intensity value of the ellipse, a is the length of the horizontal semi-axis of the ellipse, b is the length of the vertical semi-axis of the ellipse, x_0 is the x -coordinate of the centre of the ellipse, y_0 is the y -coordinate of the centre of the ellipse and ϕ is the angle (in degrees) between the horizontal semi-axis of the ellipse and the x -axis of the image.

increases. This growth corresponds to a Lyapunov exponent $\lambda \cong 0.3 > 0$, confirming chaotic behaviour (Peitgen *et al* 1992). The Lyapunov exponent was computed for $p = 2.1$, using the

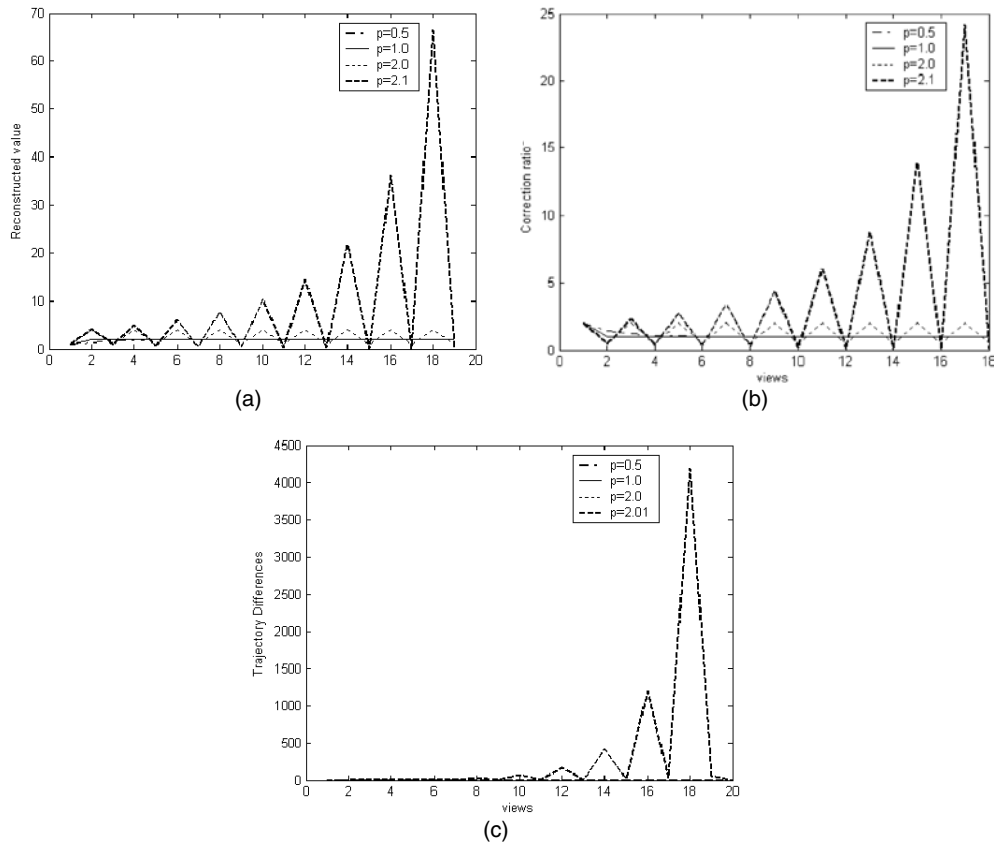


Figure 2. The reconstructed value (a) and the correction ratio (b) for the time series associated with Power MART for a single pixel image reconstructed using two views. (c) Shows the trajectory differences for two runs starting from close seeds x_0 and $x_0 + \varepsilon$, where $\varepsilon = 0.001$ and $x_0 = 1$.

expression

$$\lambda = \frac{1}{k} \ln \left(\frac{x^k(x_0 + \varepsilon) - x^k(x_0)}{\varepsilon} \right). \tag{5}$$

Chaotic behaviour is also empirically observed if we reconstruct and plot $\max(c)$, i.e., the maximum of the correction ratio for images with the number of pixels $n^2 > 1$. Figure 3 presents a logarithmic plot of $\max(c)$ for the Shepp and Logan reconstructed image with $n^2 = 157 \times 157$ and $M = 128$ views. A power $p \geq 2$ produces oscillations in the reconstruction process.

2.3. Power MART similarity to logistic equations and coupled map lattices

Power MART has behaviour similar to a logistic equation (Peitgen *et al* 1992, May 1976):

$$x^{k+1} = bx^k(1 - x^k) \tag{6}$$

with b as a parameter. To see the similarity, let us consider again the image made of a single pixel and two projections (horizontal and vertical), where the MART updating equation is

$$x^{k+1} = x^k \left(\frac{y}{x^k} \right)^p = \frac{y^p}{(x^k)^{p-1}}. \tag{7}$$

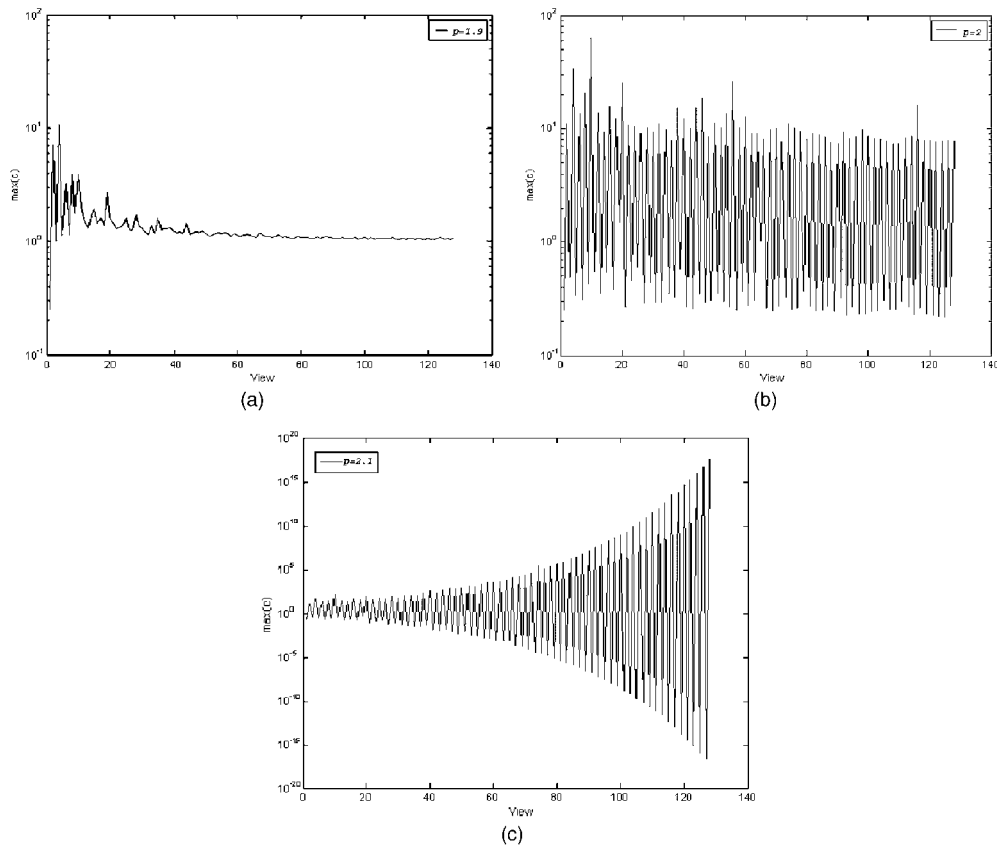


Figure 3. Logarithmic plot of the $\max(c)$ after each view (projection) is used during the first iteration. 128 views were used. (a), (b) and (c) correspond to $p = \{1.9, 2, 2.1\}$ cases, with damping (convergence to a solution of the reconstruction equations (1)), indefinite oscillations and growing oscillations, respectively.

In figure 4, we plot the logistic maps for $p = \{1.9, 2.0, 2.1\}$ using an initial seed $x^0 = 1$ and a projection $y = 2$; the x -coordinate is set as the initial value $x^0 = 1$ and a vertical line is drawn from the initial value to the ‘near’ hyperbolas (exact for $p = 2$) plotted using equation $g(x) = y^p/x^{p-1}$. The y -coordinate of the intersecting point is x^1 . This value is returned to the x -axis using the equation $g(x) = x$, and $x^2, x^3 \dots$ are obtained with the same procedure. The values of $p < 2$ produce convergence, $p = 2$ is on the edge producing oscillations between two false solutions, while $p > 2$ brings divergence.

Alternatively, by using numerical analysis (fixed point theory) we can explain the convergence/divergence property of Power MART as follows: let us use as the fixed point for the iteration $x = y = 2$; if we differentiate the iteration function in $g(x) = y^p/x^{p-1}$, and consider the values $y = 2, x^0 = 1$, we obtain the result that the iteration will be convergent locally if $(|1 - p|y^p)/x^p < 1$ for x^0 close enough to y . If x^1 is 2^p we will obtain convergence for $|1 - p| < 1$, i.e., $0 < p < 2$. There will be oscillations for $p = 2$.

Note that the recursive pixel updating in equation (2) uses the values of an anisotropic neighbourhood in the expression of c since the reprojection process $H_{ik}x^k$ involves the summation along the ray. Thus, reconstruction could be recognized as a special class of coupled map lattices (CML) (Thomas 2003) or cellular automata processes (Disconzi and Brunnet 2002). A CML is a dynamical system, in our case the image that consists of dynamical

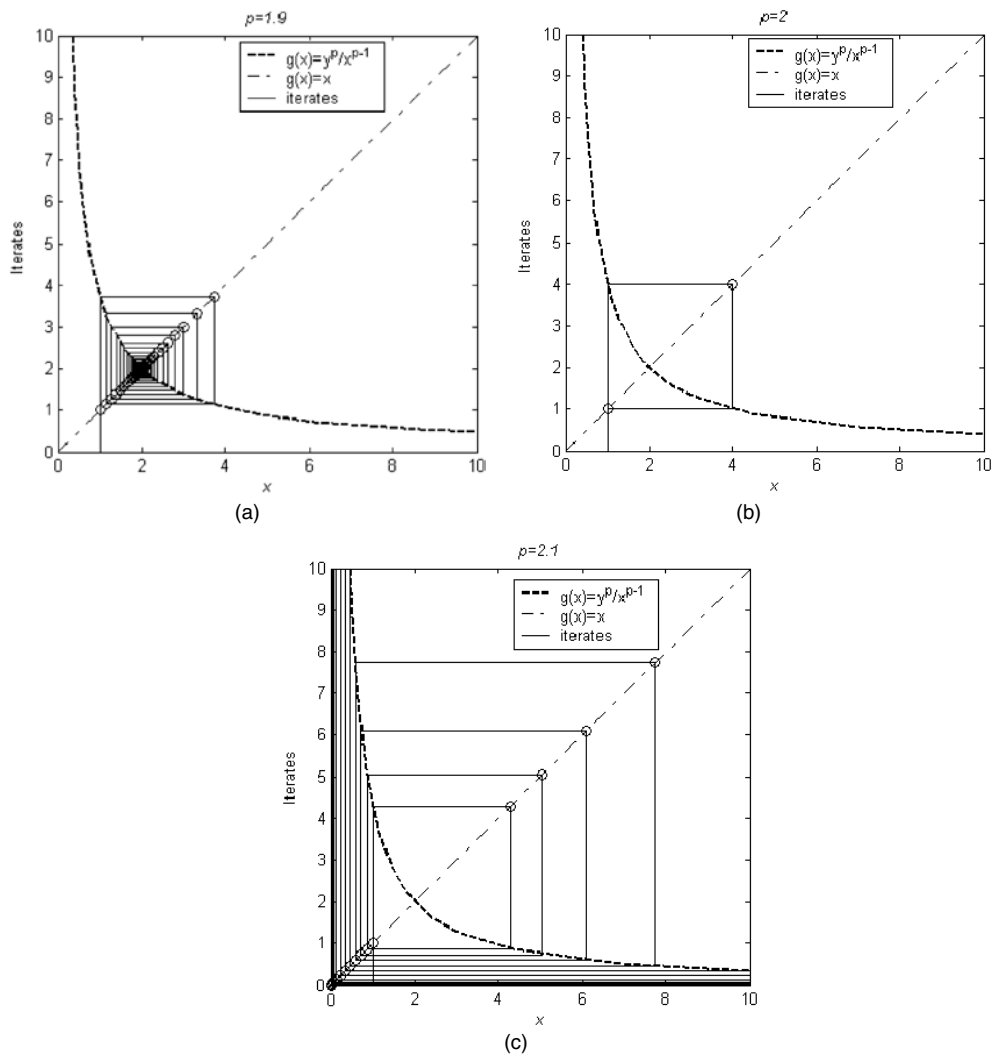


Figure 4. Logistic maps for the updating Power MART equation (4) for $p = \{1.9, 2, 2.1\}$. An initial seed $x^0 = 1$ and a projection $y = 2$ were considered; the x -coordinate is set as the initial value $x^0 = 1$ and a vertical line is drawn from the initial value to the ‘near’ hyperbolas plotted using the equation $g(x) = y^p/x^{p-1}$. The y -coordinate of the intersecting point is x^1 . This value is returned to the x -axis using the equation $g(x) = x$, and x^2, x^3, \dots are obtained with the same procedure.

elements on a lattice, i.e., the pixels, which interact with other elements on the lattice during the iterative process. The neighbourhoods on which the pixels interact, i.e., the rays in this CML model, change from one view (angle) to another.

2.4. Power MART performance versus exponent

As will be shown by our results (see figures 5–8), the nonlinearity introduced by the different p exponents in Power MART can improve the figures of merit (FOMs) when compared to the original MART algorithm, for noise-free data. Two types of phantoms were used for assessment, i.e., the Shepp and Logan (figures 5 and 6) phantom and a CT image phantom

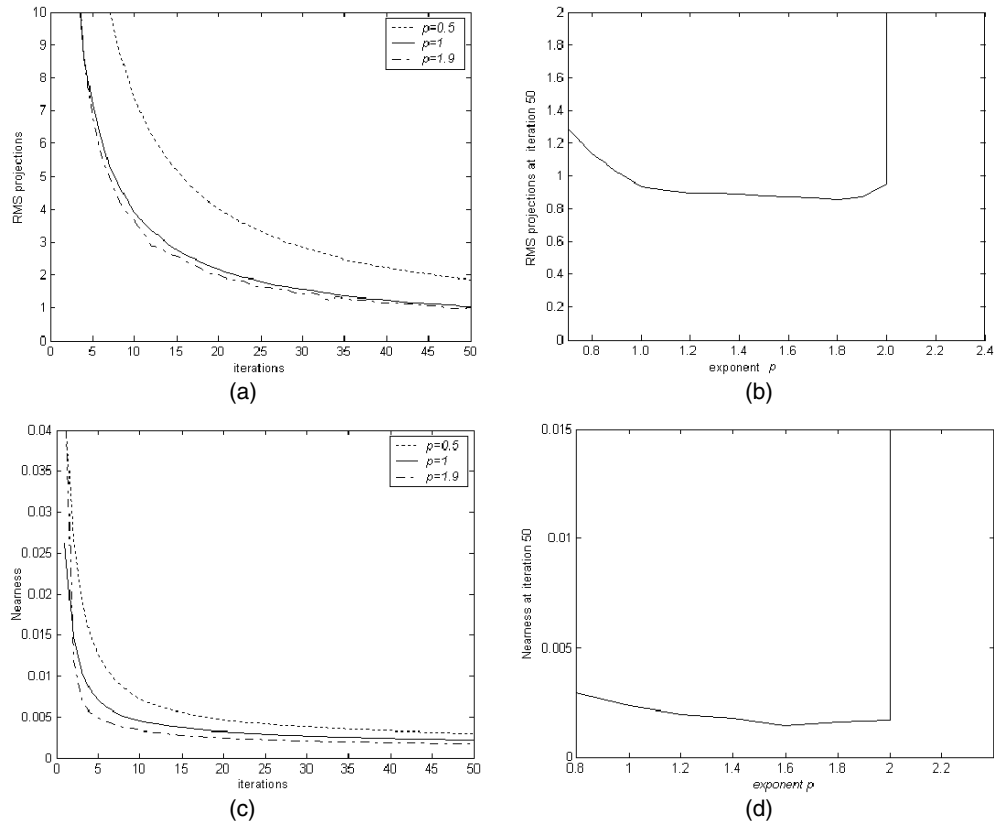


Figure 5. The Shepp and Logan phantom: Power MART performances versus the exponent p for noise-free projections and the Shepp and Logan phantom. The RMS for projections (a) and the nearness (c) were computed for $p = \{0.5, 1, 1.9\}$ and displayed during the first 50 iterations. In (b) and (d) the RMS and nearness at iteration 50 versus the p exponent are plotted; p was varied in increments of 0.1.

(figures 7 and 8). Both noiseless and noisy projections with different SNR = {10, 20, 50} were used. For image quality assessment we used two FOMs:

- The root mean square (RMS) distance in Euclidean ($M \times n$)-dimensional space between the projection and the original projections:

$$\text{RMS}_k = \sqrt{\sum_{i=1}^{M \times n} (y_i - H_{ik} x^k)^2}. \quad (8)$$

- The overall nearness FOM as given by Gordon and Herman (1974). This is the RMS distance in Euclidean n^2 -dimensional space between the reconstruction and the original, normalized by the standard deviation of the original. The expression for the nearness FOM is given by

$$\delta' = \left| \frac{\sum_{j=1}^{n^2} (x_j - x_j^0)^2}{\sum_{j=1}^{n^2} (x_j^0 - \bar{x}^0)^2} \right| \quad (9)$$

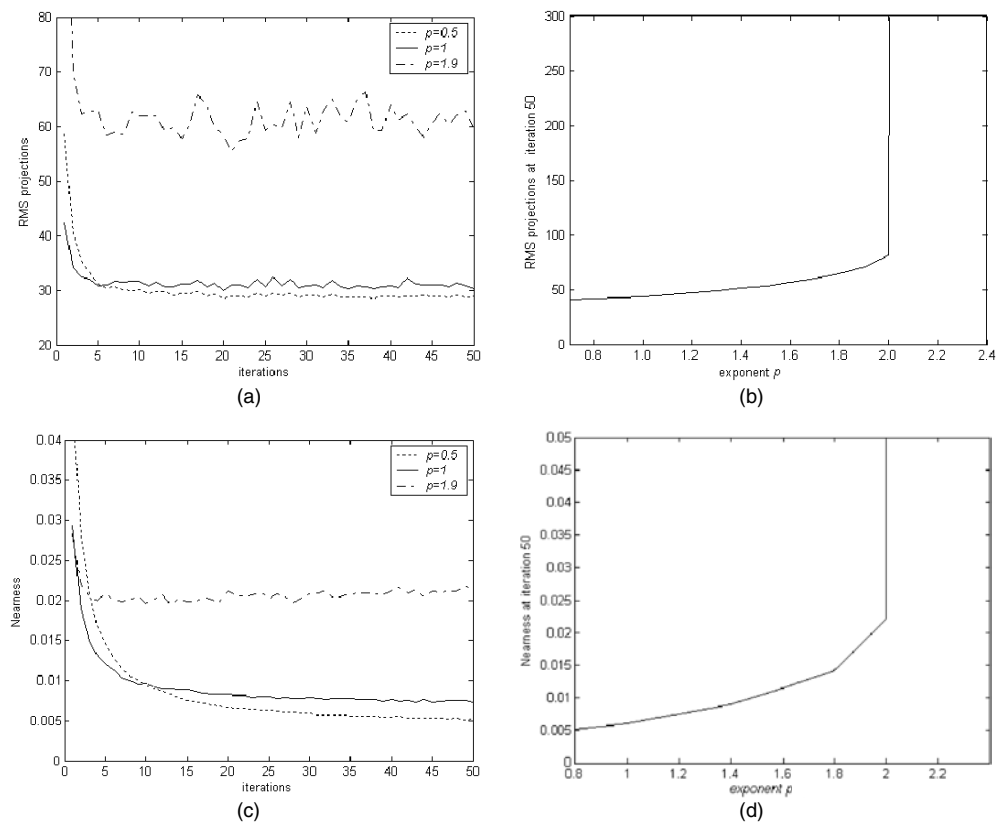


Figure 6. The Shepp and Logan phantom: Power MART performances versus the exponent p for noisy projections (SNR = 20). The RMS for projections (a) and the nearness (c) were computed for $p = \{0.5, 1, 1.9\}$ and displayed during the first 50 iterations. In (b) and (d) the RMS and nearness at iteration 50 versus the p exponent are plotted; p was varied in increments of 0.1.

where x and x^0 refer to the reconstructed and the original test image; \bar{x}^0 is the mean value of the test image.

A lower RMS of the projections would ensure a better agreement between the reconstructed image (the solution of the inverse problem) and the available, measured projections. A lower nearness FOM would also account for a better similarity to the phantom image.

2.5. Boxcar averaging MART

Boxcar averaging refers to the practice of averaging the outputs over the previous B observations in an experiment. We investigated whether the chaotic behaviour would be affected by averaging solutions between projections with $B = 2$. Insight into the boxcar effect is again obtained by studying the logistic maps. As shown by figure 9(a), boxcar averaging removes the cycling and ensures convergence at $p = 2$ but does not remove the chaotic behaviour at higher exponents such as $p = 5$ (see figure 9(b)), where the image is brought close to a solution and then diverges from it. This is also confirmed by the RMS plots (figure 9(c)) computed for reconstructed images of the Shepp and Logan phantom with

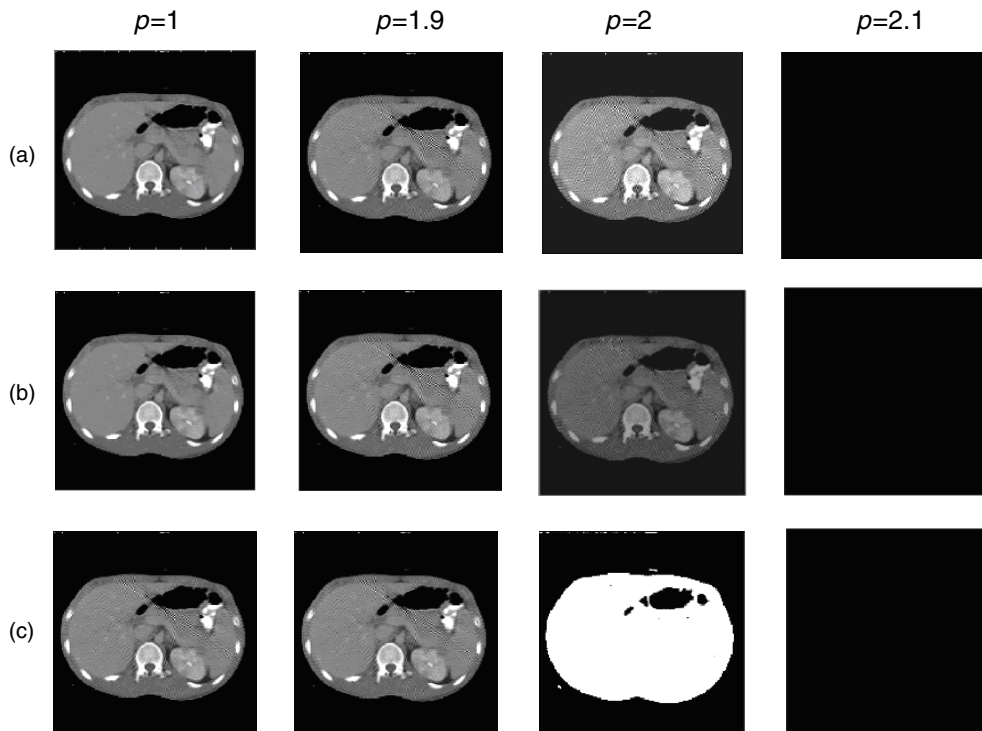


Figure 7. The CT image phantom: Power MART reconstructions for $p = \{1, 1.9, 2, 2.1\}$ after first (a), fifth (b) and tenth (c) iterations. Note that $p < 2$ converges, $p = 2$ cycles between two false solutions shown here at iterations 5 (b) and 10 (c), while $p = 2.1$ causes the collapse of the image even before iteration 1.

$n^2 = 157 \times 157$ and $M = 128$ projections. Empirically, the critical power for Boxcar Averaging MART was close to $p_c = 4$.

2.6. Bouncing MART

If, during the reconstruction process, we monitor the convergence rate computed as $r_k = \frac{|\text{RMS}_k - \text{RMS}_{k-1}|}{\text{RMS}_k}$ with k as the iteration number, we could use the low values of r_k to ‘shake’ the reconstruction process. Thus, we propose the ‘Bouncing MART’ algorithm in which $p = 2$ if $r_k < a/k$ (to ‘bounce’ the image) and $p = 1$ when $r_k \geq a/k$ (to let it converge). This has two justifications: (a) bouncing is analogous to simulated annealing (Laarhoven and Aarts 1987, Mazur *et al* 1993); (b) in the case of underdetermined equations, bouncing provides a new way of exploring the hyperplane of alternative solutions (Gordon 1973). Simulated annealing was successfully applied in optimization problems where an iterative procedure is used to find the optimum solution. Iterative improvements consist of a search ‘downhill’ in the solutions space. The search usually gets stuck in a local minimum. One way of solving this problem is to start from different randomly generated configurations, carry out the process and save the best results. Simulated annealing introduced an alternative method that ‘shakes’ the procedure from a local optimum by pushing sometimes ‘uphill’ and then ‘downhill’. It is the same idea that we use in the Bouncing MART although our scope is not to find a global minimum but a better image. If this is achieved, we believe that we are indeed coming close to the global optimum solution. By changing the p values and introducing the oscillations $p = 2$ for short

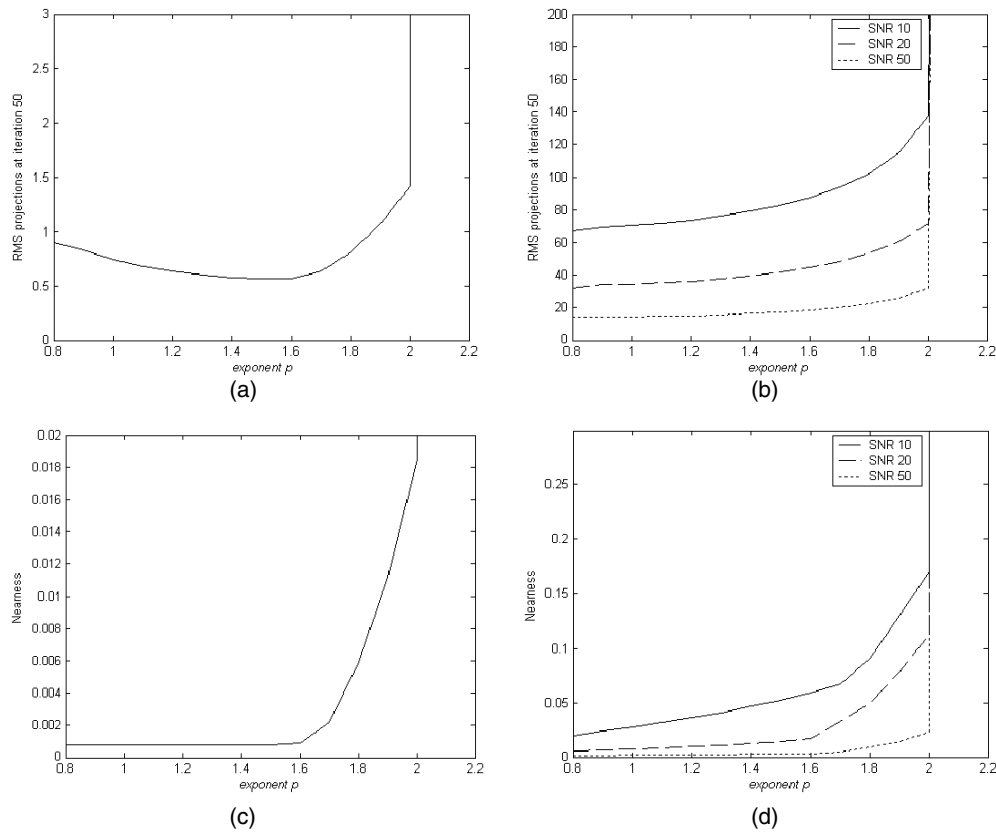


Figure 8. The CT image phantom: Power MART performances versus the exponent p for noise-free (a), (c) and noisy projections (b), (d). The RMS for projections and the nearness at iteration 50 were computed versus the p exponent. In (b) and (d) the RMS and nearness are plotted for SNR = {10, 20, 50}; p was varied in increments of 0.1.

time we move ‘uphill’ away from a solution. $p = 1$ allows the ‘downhill’ recovery of the algorithm. The decrease in threshold with k is analogous to the decrease in pseudotemperature in simulated annealing. The parameter a is introduced to control the number and the instances of the bouncing occurrences during the reconstruction process. Thus, $a > 1$ will increase the frequency of bouncing while $a < 1$ will reduce it, allowing more recovery iterations with $p = 1$.

2.7. Simulations of Bouncing MART

The performance of Bouncing MART versus original MART has been ascertained using perfect and noisy parallel projection data of the modified Shepp and Logan phantom. We studied the algorithm for various situations, including limited number of views or limited arc reconstruction. Our experimental comparisons span the following cases for reconstructing an image with $n^2 = 157 \times 157$ unknowns:

- (a) a well-determined case (full arc, $M = 128$ equally spaced views, with angle step = 1.4063°), i.e., $M \times n = 128 \times 157$ equations;
- (b) a highly underdetermined case (full arc, $M = 16$ equally spaced views, angle step = 11.2504°), i.e., $M \times n = 16 \times 157$ equations; and

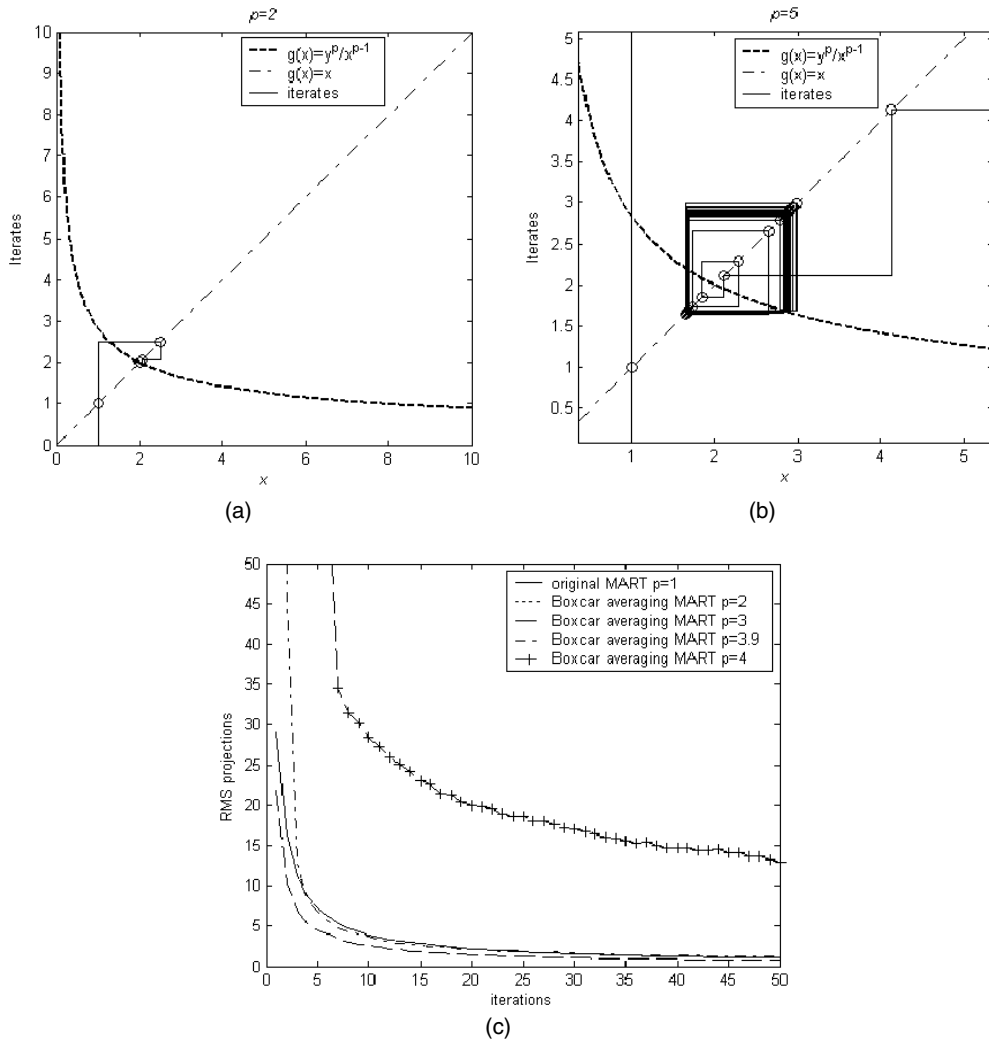


Figure 9. Boxcar Averaging MART. The logistic maps for the Boxcar Averaging MART equation for $p = 2$ (a) and $p = 5$ (b). (c) Presents the RMS computed in reconstructions of a Shepp and Logan phantom with $n^2 = 157 \times 157$ with $M = 128$ views for the original MART, i.e., $p = 1$, and the Boxcar Averaging MART with $p = \{2, 3, 3.9, 4\}$. The RMS for Boxcar Averaging MART with $p = 5$ is off scale and thus not shown.

(c) a limited arc, underdetermined case ($M = 64$ equally spaced views, acquired over an arc of 90° , with angle step = 1.4063°), i.e., $M \times n = 64 \times 157$ equations.

Since the reconstruction algorithms address inversion of ill-conditioned matrices, it is reasonable to expect their sensitivity to noise. The main source of noise in x-ray projection data is quantum noise. The number of photons passing through the patient and striking the detectors is susceptible to quantum fluctuations, and is given by

$$N = N_0 \exp\left(-\int_l x dl\right) \tag{10}$$

where N_0 and N are the mean number of photons before and after passing through the object and the integral is computed along each ray l . A common measure of the image quality is the

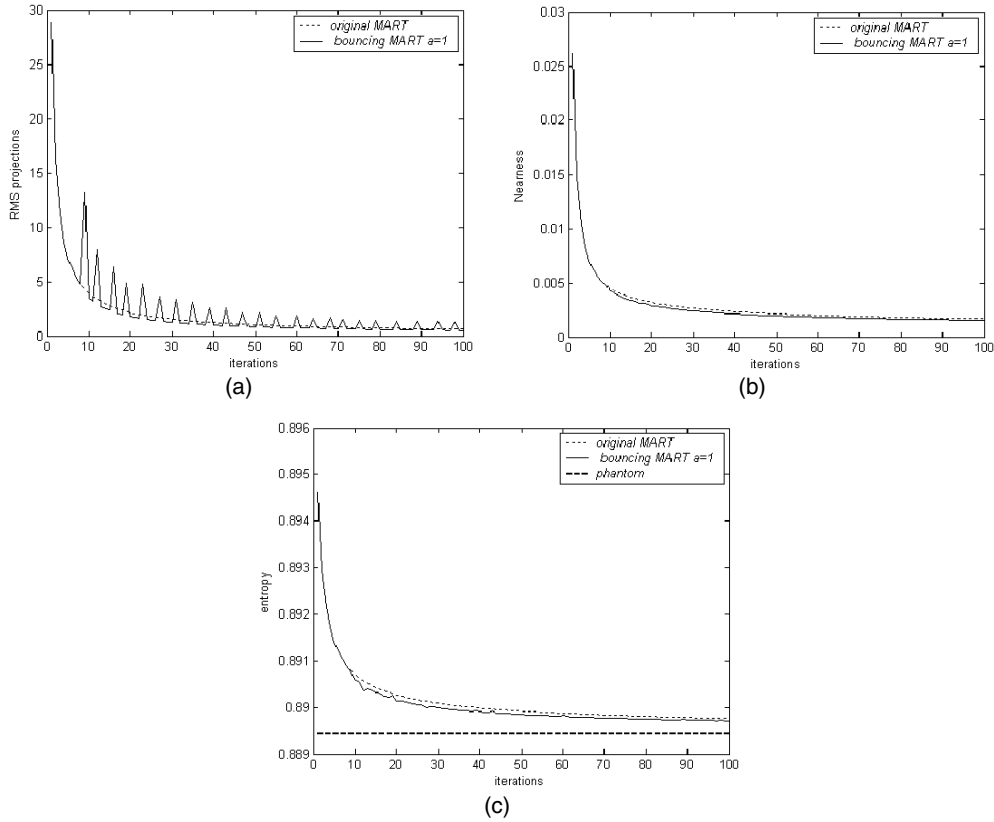


Figure 10. Bouncing MART performances. The RMS of the projections (a), the nearness FOM (b) and the entropy (c) for the well-determined case, i.e., $n^2 = 157 \times 157$, with $M = 128$ equally distributed projections over 180° .

signal (S) to noise (σ) ratio (SNR), which is dependent on the number of photons N , assuming Poisson statistics, according to the relation

$$\text{SNR} = \frac{S}{\sigma} \cong \frac{N}{\sqrt{N}} = \sqrt{N}. \quad (11)$$

A $\text{SNR} = 20$ in the projection data affected by Poisson noise was used with all the Bouncing MART algorithm variations.

The weighted distance scheme (WDS) for projection ordering (Mueller *et al* 1997) was performed during all reconstruction procedures. WDS heuristically attempts to optimize the order of projections therefore ensuring a great speed of convergence and accuracy of the reconstruction, as we have also demonstrated (Guan and Gordon 1996).

2.8. Assessment of image quality

In order to quantitatively compare the reconstructed images and to evaluate the performance of the algorithms, the following measures were computed:

- (a) The RMS for projections computed to measure the error between the projections and reprojections, as in equation (8).
- (b) The overall nearness FOM as given in equation (9).

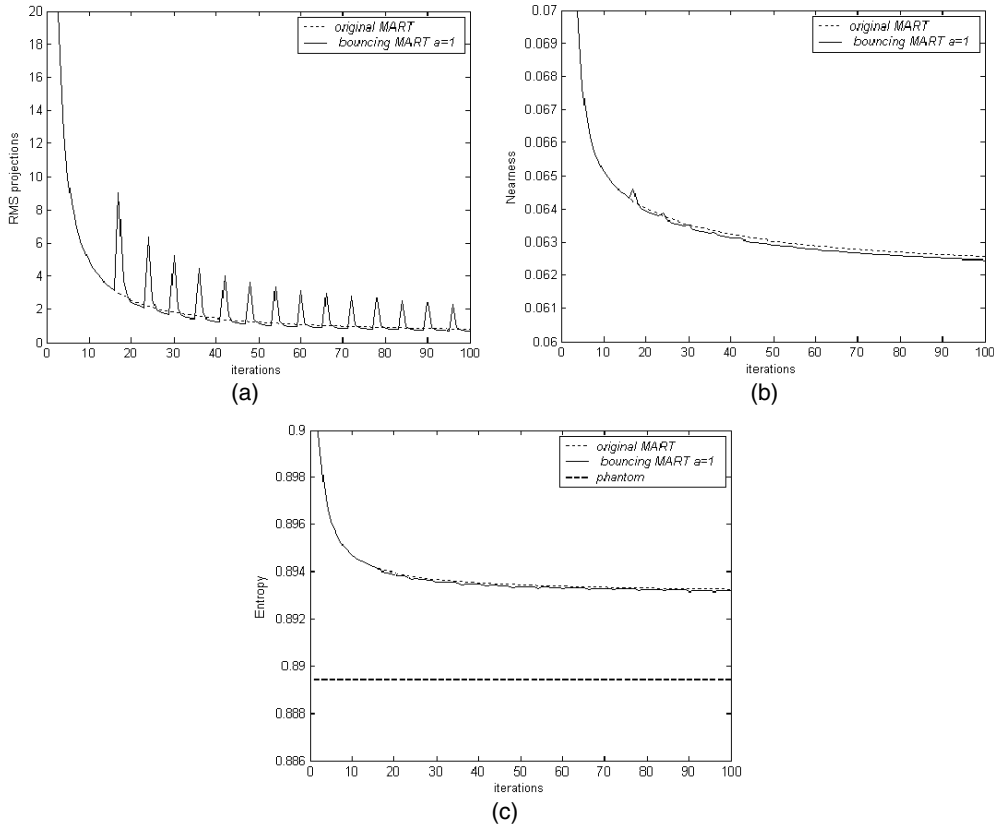


Figure 11. Bouncing MART performances for limited number of views. The RMS of the projections (a), the nearness FOM (b) and the entropy (c) for the limited number of views case, i.e., $n^2 = 157 \times 157$, $M = 16$ projections equally distributed projections over 180° .

(c) The entropy S given, as in Gordon *et al* (1970), by equation

$$S = \frac{-1}{\ln n^2} \sum_{j=1}^{n^2} \left(\frac{x_j}{\tau} \right) \ln \left(\frac{x_j}{\tau} \right) \quad (12)$$

where n^2 is the size of the reconstructed image, x_j is the image value at pixel j and τ is the total density of the reconstructed image, which is evaluated using any of the available projections y :

$$\tau = \sum_{i=1}^P y_i$$

(applicable to parallel projections) where P is the total number of rays in projection y .

3. Results

The performance of Power MART versus the exponent p was explored for the well-determined case $M = 128$ using Shepp and Logan (figures 5 and 6) and CT image phantoms (figures 7 and 8). Both noise-free and noisy projections were used. With the CT phantom image ($n^2 = 157 \times 157$) the influence of different SNRs (SNR = {10, 20, 50}) was studied (see

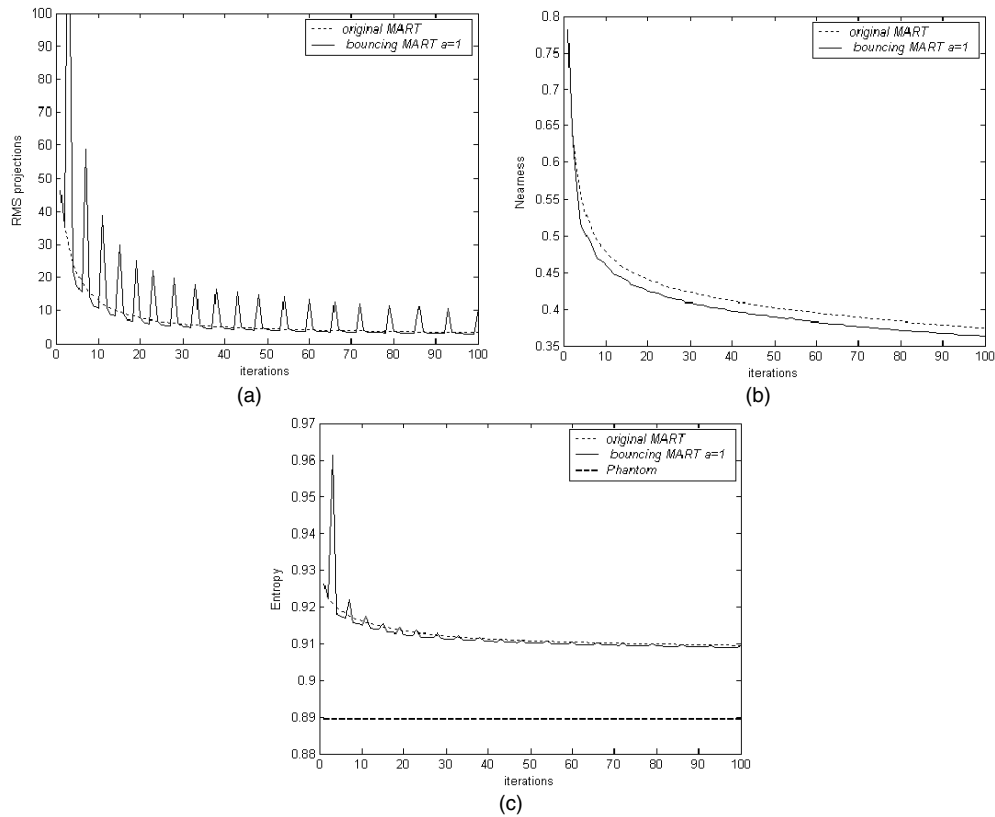


Figure 12. Bouncing MART performances for the limited angle case. The RMS of the projections (a), the nearness FOM (b) and the entropy (c) for the limited angle case, i.e., $n^2 = 157 \times 157$, $M = 16$ projections equally distributed projections over 90° .

figure 8). Using the noise-free dataset, figure 9(c) presents the RMS computed for the original MART, i.e., $p = 1$, and the Boxcar Averaging MART with different values of p . Note that two plots are almost overlain, i.e., Boxcar Averaging MART with $p = 2$ provides almost identical RMS values as the original MART and does not improve the reconstruction process; note also that $p = \{2, 3, 3.9\}$ provided better RMS than $p = 4$. The RMS for Boxcar Averaging MART with $p = 5$ reached huge values and could not be plotted on the same graph due to the differences in scale. Figures 10–14 refer to the Bouncing MART performance evaluated using all the computed FOMs. Thus, figures 10–12 present the results for the noise-free dataset for the well-determined (figure 10) limited number of views (figure 11), and limited angle (figure 12) cases. Figure 13 shows the same FOMs for the noisy, well-determined dataset. Since $a = 1$ used in the Bouncing MART did not produce better FOMs for the noisy dataset, we experimented with different values of a and the results are shown in figure 13. We also investigated whether a higher value $p = 2.1$ would improve the reconstruction process in Bouncing MART both for noise-free and noisy datasets. The results are given in figure 14.

4. Discussion

The different exponents of the correction terms applied in all Power MART variations affect the reconstructed images in an interesting way. As shown by our results, both Power MART

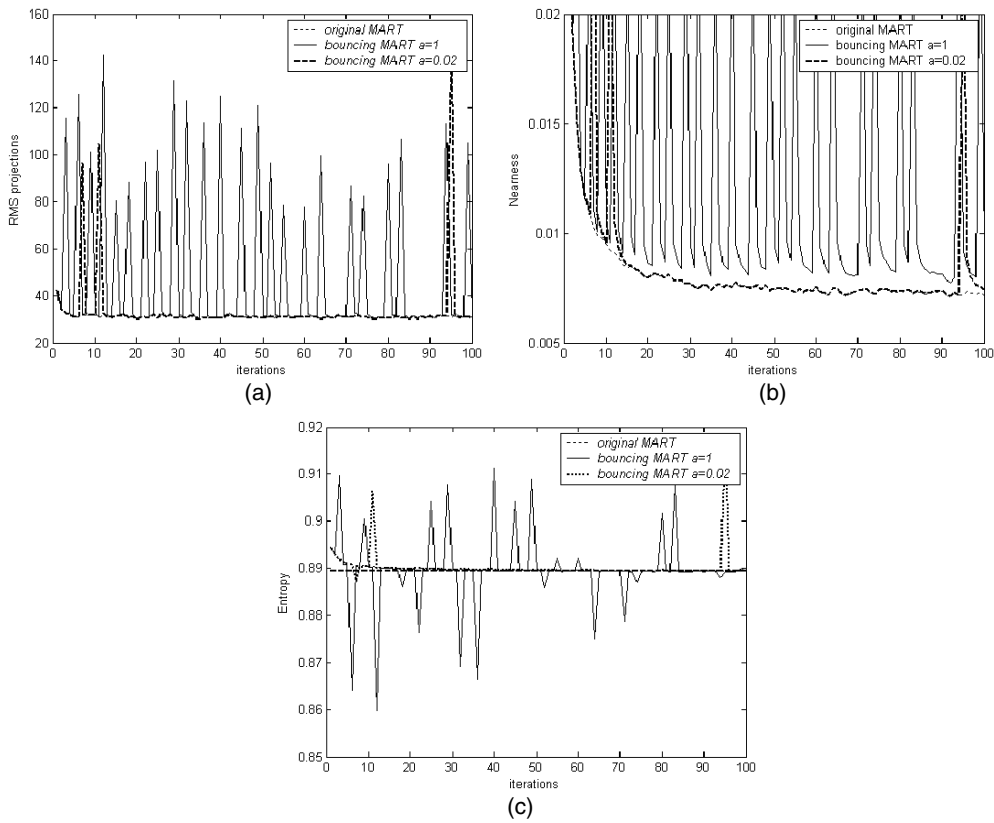


Figure 13. Bouncing MART performances in the case of noisy projections. The RMS of the projections (a), the nearness FOM (b) and the entropy (c) for the noisy, well-determined case $n^2 = 157 \times 157$, $M = 128$ projections equally distributed over 180° with $SNR = 20$.

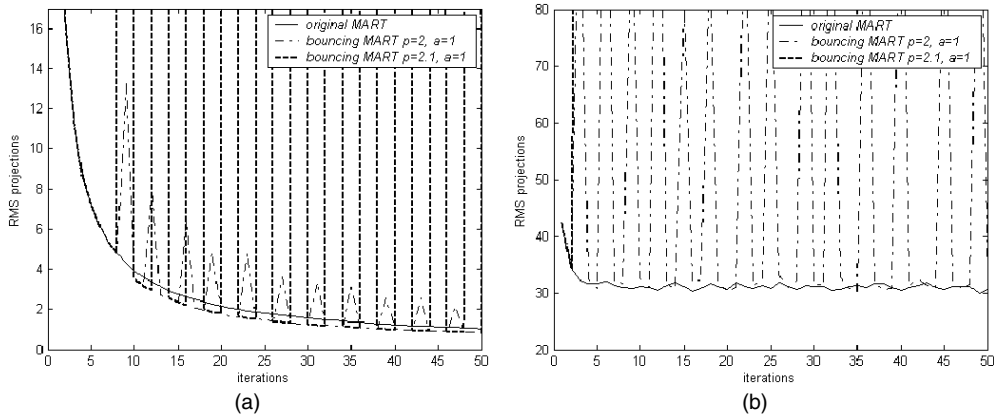


Figure 14. The RMS of the projections for bouncing MART with $p = \{1, 2, 2.1\}$ with noise-free (a) and noisy projections $SNR = 20$ (b) for the well-determined case $n^2 = 157 \times 157$, $M = 128$ projections equally distributed over 180° .

and Bouncing MART with $2 > p > 1$ are able to provide better FOMs (RMS projections and nearness) when compared to the original MART for noise-free data. The exponents

ensure lower FOMs for those cases of reconstructions. This was shown to be independent of the image content (see figures 5–9). Power MART performance can improve for values of $p < p_c = 2$, perhaps a case of approaching the ‘edge of chaos’ (Kauffman and Johnsen 1991, Langton 1992, Lewin 1992, Waldrop 1992, Ray and Jan 1994, Smith 1995). The term ‘edge of chaos’ refers in our case to the critical power $p = 2$ which separates convergence via oscillations from divergence. In our case the divergence could be associated with chaos as shown by the positive Lyapunov parameter. The reverse happens in the presence of clinical levels of noise (see figures 5(c) and (d)) where $p < 1$ actually shows better results than the original MART.

The benefit of Bouncing MART with a noiseless dataset is also reflected by the entropies of the reconstructed images, which in these cases are closer to the entropy of the original phantom. Noisy projections contravene the performance of Bouncing MART (figure 13). Changing the parameter a , which controls the bouncing occurrences, to the range $a \ll 1$, provides results that are not better than the original MART. Values of $p > 2$ in Bouncing MART do not improve the RMS of projections (see figure 14 for $p = 2.1$). Empirically, values of $p > 2$ bring the collapse of the Bouncing MART reconstruction process, a bit higher than $p_c = 2$ for Power MART.

5. Conclusion

We presented and evaluated variations of the MART algorithm. The reason such variations produce different images is that we are applying them to underdetermined sets of CT equations, so that an infinite number of alternative solutions is available. We use underdetermined equations because this is the simplest way to reduce the number of equations, and thus the x-ray dose. It has long been known that ART and other iterative algorithms produce significantly superior images to the commonly used Fourier backprojection algorithm when the number of views is reduced so that the equation sets are highly underdetermined (Barbieri 1974, Herman 1980). Our investigations prove that there is scope to optimize CT algorithms and thereby achieve greater dose reduction. We have shown that increasing the nonlinearity of a nonlinear computed tomography algorithm can enhance the accuracy of the reconstructed image for noise-free data. The reconstruction accuracy improvements conform to the general notion that regularization as a means of solving simultaneous linear equations that are underdetermined does not necessarily select the correct image from the hyperplane of solutions (Gordon 1973). Additive ART minimizes image variance (Gordon and Herman 1974), MART maximizes entropy (Lent 1977, Lent and Censor 1991) and FBP selects the pseudoinverse (Anastasio *et al* 2001), so all three basic algorithms are routes to generally suboptimal, regularized solutions of the projection equations (1), i.e., *regularization as a means to finding the optimal solution to a set of simultaneous equations in general leads to suboptimal results*. We believe that the optimal stochastic solution should converge to the optimal deterministic solution, when photon counts are high, which means that once we have achieved the optimal deterministic solution, we will know better how to handle the stochastic case (Leahy and Byrne 2000, De Man *et al* 2001, Elbakri and Fessler 2002). Geometric deconvolution (Dhawan *et al* 1984a, 1984b, 1984c, Dhawan *et al* 1985, Rangayyan *et al* 1985) finds significantly better images than those resulting from regularization. Our failure to gain improvement with noisy data suggests that increasing nonlinearity may be antagonistic to noise suppression. Nevertheless, some middle ground may be anticipated. Thus the next step in our efforts to squeeze as much information out of CT data as possible, to maximize the image quality:dose ratio, will be to combine Power MART with geometric deconvolution, which has been shown to substantially improve image quality for CT with a limited angle range and number of

projections (Dhawan *et al* 1985). Since the nonlinearity in Power MART and geometric deconvolution both generally amplify noise, a subtle balance must be sought.

Acknowledgments

We would like to acknowledge the Duke Center for In Vivo Microscopy, an NIH/NCRR National Resource (P41 RR05959), and the Department of Defense (DAMD 17-02-2-0004). We would also like to thank 'Friends You Can Count On' for a grant for dose reduction in breast CT, and the Manitoba Institute for Child Health for partial support in the form of a grant for reducing paediatric CT dose. Critical comments by G Allan Johnson, Alvaro R De Pierro, Gabor Herman and Yair Censor and the referees, and illuminating conversations with Andrew Jason Penner, were most appreciated.

References

- Anastasio M A, Pan X and Clarkson E 2001 Comments on the filtered backprojection algorithm, range conditions, and the pseudoinverse solution *IEEE Trans. Med. Imaging* **20** 539–42
- Badea C T 2000 Volume imaging using a combined cone beam CT-DTS approach *PhD Thesis* University of Patras, Greece (available on line at <http://bme.med.upatras.gr/bit/>)
- Barbieri M 1974 A criterion to evaluate three dimensional reconstructions from projections of unknown structures *J. Theor. Biol.* **48** 451–67
- Beyer W A and Ulam S M 1968 Note on the visual hull of a set *J. Comb. Theory* **4** 240–5
- Browne J and De Pierro A 1996 A row-action alternative to the EM algorithm for maximizing likelihoods in emission tomography *IEEE Trans. Med. Imaging* **15** 687–99
- Censor Y, De Pierro A, Elfving T, Herman G T and Iusem A 1989 On iterative methods for linearly constrained entropy maximization *Numer. Anal. Math. Modelling* **5** 147–65
- Chaudhuri B B and Rosenfeld A 1998 On the computation of the digital convex hull and circular hull of a digital region *Pattern Recognit.* **31** 2007–16
- Chlewicki W 2001 *3D Simultaneous Algebraic Reconstruction Technique for Cone-Beam Projections* (Patras: University of Patras)
- Cho Z H, Wu E X and Hilal S K 1994 Weighted backprojection approach to cone beam 3D projection reconstruction for truncated spherical detection geometry *IEEE Trans. Med. Imaging* **13** 110–21
- Crawley M T, Booth A and Wainwright A 2001 A practical approach to the first iteration in the optimization of radiation dose and image quality in CT: estimates of the collective dose savings achieved *Br. J. Radiol.* **74** 607–14
- Daroch J N and Ratcliff D 1972 Generalized iterative scaling for log-linear models *Ann. Math. Stat.* **43** 1470–80
- De Man B, Nuyts J, Dupont P, Marchal G and Suetens P 2001 An iterative maximum-likelihood polychromatic algorithm for CT *IEEE Trans. Med. Imaging* **20** 999–1008
- De Pierro A and Iusem A 1986 A relaxed version of Bregman's method for convex programming *J. Optim. Theory Appl.* **51** 421–40
- Defrise M and Clack R 1994 A cone-beam reconstruction algorithm using shift-variant filtering and cone-beam backprojection *IEEE Trans. Med. Imaging* **13** 186–95
- Dhawan A P, Rangayyan R M and Gordon R 1984a Wiener filtering for deconvolution of geometric artifacts in limited-view image reconstruction *Proc. SPIE* **515** 168–72
- Dhawan A P, Rangayyan R M and Gordon R 1984b Image restoration by two-dimensional deconvolution in limited-view reconstruction *Topical Meeting on Industrial Applications of Computed Tomography and NMR Imaging (Hecla Island, Canada)*
- Dhawan A P, Rangayyan R M and Gordon R 1984c Image restoration by deconvolution in computed tomography *Scientific Exhibits at Annual Meeting of Radiological Society of North America (Washington, DC)*
- Dhawan A P, Rangayyan R M and Gordon R 1985 Image restoration by Wiener deconvolution in limited-view computed tomography *App. Opt.* **24** 4013–20
- Disconzi M and Brunnet L 2002 Non-linear dynamics: models to the formation of spatio-temporal structures *I Colóquio Interdisciplinar de Dinâmica-UFRGS-2002*
- Donaire J G and Garcia I 1999 On improving the performance of ART in 3D cone beam transmission tomography *Proc. of the 1999 International Meeting on Fully 3D Image Reconstruction in Radiology and Nuclear Medicine*

- Donnelly L F, Emery K H, Brody A S, Laor T, Gylys-Morin V M, Anton C G, Thomas S R and Frush D P 2001 Minimizing radiation dose for pediatric body applications of single-detector helical CT: strategies at a large Children's Hospital *AJR Am. J. Roentgenol.* **176** 303–6
- Elbakri I A and Fessler J A 2002 Statistical image reconstruction for polyenergetic X-ray computed tomography *IEEE Trans. Med. Imaging* **21** 89–99
- Giacomuzzi S M, Erckert B, Schopf T, Freund M C, Springer P, Dessl A and Jaschke W 1996 The smart-scan procedure of spiral computed tomography A new method for dose reduction *Rofo Fortschr Geb Rontgenstr Neuen Bildgeb Verfahr* **165** 10–6
- Gordon R 1973 Artifacts in reconstructions made from a few projections *1st Int. Joint Conf. on Pattern Recognition (Washington, DC)*
- Gordon R 1976 Dose reduction in computerized tomography (Guest Editorial) *Invest. Radiol.* **111** 508–17
- Gordon R, Bender R and Herman G T 1970 Algebraic reconstruction techniques (ART) for three-dimensional electron microscopy and x-ray photography *J. Theor. Biol.* **29** 471–81
- Gordon R and Herman G T 1974 Three dimensional reconstruction from projections: a review of algorithms *Int. Rev. Cytol.* **38** 111–51
- Greess H, Baum U, Wolf H, Lell M, Nomayr A, Schmidt B, Kalender W A and Bautz W 2001 Dose reduction in spiral-CT: detection of pulmonary coin lesions with and without anatomically adjusted modulation of tube current *Rofo Fortschr Geb Rontgenstr Neuen Bildgeb Verfahr* **173** 466–70
- Greess H, Nomayr A, Wolf H, Baum U, Lell M, Bowing B, Kalender W and Bautz W A 2002 Dose reduction in CT examination of children by an attenuation-based on-line modulation of tube current (CARE Dose) *Eur. Radiol.* **12** 1571–6
- Greess H, Wolf H, Baum U, Kalender W A and Bautz W 1999 Dosage reduction in computed tomography by anatomy-oriented attenuation-based tube-current modulation: the first clinical results *Rofo Fortschr Geb Rontgenstr Neuen Bildgeb Verfahr* **170** 246–50
- Greess H, Wolf H, Baum U, Lell M, Pirkel M, Kalender W and Bautz W A 2000 Dose reduction in computed tomography by attenuation-based on-line modulation of tube current: evaluation of six anatomical regions *Eur. Radiol.* **10** 391–4
- Guan H and Gordon R 1996 Computed tomography using Algebraic Reconstruction Techniques (ARTs) with different projection access schemes: a comparison study under practical situations *Phys. Med. Biol.* **41** 1727–43
- Herman G T 1980 *Image Reconstruction from Projections. The Fundamentals of Computerized Tomography* (San Francisco: Academic)
- Hsieh J, Molthen R C, Dawson C A and Johnson R H 2000 An iterative approach to the beam hardening correction in cone beam CT *Med. Phys.* **27** 23–9
- Itoh S, Koyama S, Ikeda M, Ozaki M, Sawaki A, Iwano S and Ishigaki T 2001 Further reduction of radiation dose in helical CT for lung cancer screening using small tube current and a newly designed filter *J. Thorac. Imaging* **16** 81–8
- Kachelriess M, Watzke O and Kalender W A 2001 Generalized multi-dimensional adaptive filtering for conventional and spiral single-slice, multi-slice, and cone-beam CT *Med. Phys.* **28** 475–90
- Kalender W 2000 *Computed Tomography: Fundamentals, System Technology, Image Quality, Applications* (Munich: Publicis MCD Verlag)
- Kalender W A, Wolf H, Suess C, Gies M, Greess H and Bautz W A 1999 Dose reduction in CT by on-line tube current control: principles and validation on phantoms and cadavers *Eur. Radiol.* **9** 323–8
- Kalra M K, Prasad S, Saini S, Blake M A, Varghese J, Halpern E F and Thrall J H 2002 Clinical comparison of standard-dose and 50% reduced-dose abdominal CT: effect on image quality *AJR Am. J. Roentgenol.* **179** 1101–6
- Kauffman S A and Johnsen S 1991 Coevolution to the edge of chaos: coupled fitness landscapes, poised states, and coevolutionary avalanches *J. Theor. Biol.* **149** 467–505
- Kudo H, Noo F and Defrise M 1998 Cone-beam filtered-backprojection algorithm for truncated helical data *Phys. Med. Biol.* **43** 2885–909
- Kudo H, Noo F and Defrise M 2000 Quasi-exact filtered backprojection algorithm for long-object problem in helical cone-beam tomography *IEEE Trans. Med. Imaging* **19** 902–21
- Kudo H and Saito T 1998 Fast and stable cone-beam filtered backprojection method for non-planar orbits *Phys. Med. Biol.* **43** 747–60
- Laarhoven P J M and Aarts E H L 1987 *Simulated Annealing: Theory and Applications* (Norwell, MA: Kluwer)
- Langton C G 1992 Life at the edge of chaos *Artificial Life II* ed C G Langton, C Taylor, J D Farmer and S Rasmussen (Reading, MA: Addison-Wesley) pp 41–91
- Leahy R and Byrne C 2000 Recent developments in iterative image reconstruction for PET and SPECT *IEEE Trans. Med. Imaging* **19** 257–60
- Lehmann K J, Wild J and Georgi M 1997 Clinical use of software-controlled x-ray tube modulation with 'Smart-Scan' in spiral CT *Aktuelle. Radiol.* **7** 156–8

- Lent A 1977 A convergent algorithm for maximum entropy image restoration, with a medical x-ray application *Image Analysis and Evaluation* ed R Shaw (Washington, DC: Society of Photographic Scientists and Engineers) pp 249–57
- Lent A and Censor Y 1991 The primal-dual algorithm as a constraint-set-manipulation device *Math. Program.* **50** 343–57
- Lewin R 1992 *Complexity: Life at the Edge of Chaos* (New York: Macmillan)
- Mastora I, Remy-Jardin M, Suess C, Scherf C, Guillot J P and Remy J 2001 Dose reduction in spiral CT angiography of thoracic outlet syndrome by anatomically adapted tube current modulation *Eur. Radiol.* **11** 590–6
- May R M 1976 Simple mathematical models with very complicated dynamics *Nature* **261** 459–67
- Mazur A K, Mazur E J and Gordon R 1993 Digital differential radiography (DDR): a new diagnostic procedure for locating neoplasms, such as breast cancers, in soft, deformable tissues *Proc. SPIE* **1905** 443–55
- Meisters G H and Ulam S M 1967 On visual hulls of sets *Proc. Natl. Acad. Sci. USA* **57** 1172–4
- Mueller K, Chang J, Amols H and Ling C C 2000 Cone-beam computed tomography (CT) for a megavoltage linear accelerator (LINAC) using an electronic portal imaging device (EPID) and the algebraic reconstruction technique (ART) *Annual Int. Conf. of the IEEE Engineering in Medicine and Biology Society (Chicago, IL)*
- Mueller K and Yagel R 2000 Rapid 3-D cone-beam reconstruction with the simultaneous algebraic reconstruction technique (SART) using 2-D texture mapping hardware *IEEE Trans. Med. Imaging* **19** 1227–37
- Mueller K, Yagel R and Cornhill J F 1997 The weighted-distance scheme: a globally optimizing projection ordering method for ART *IEEE Trans. Med. Imaging* **16** 223–30
- Mueller K, Yagel R and Wheller J J 1999a Anti-aliased three-dimensional cone-beam reconstruction of low-contrast objects with algebraic methods *IEEE Trans. Med. Imaging* **18** 519–37
- Mueller K, Yagel R and Wheller J J 1999b Fast implementations of algebraic methods for three-dimensional reconstruction from cone-beam data *IEEE Trans. Med. Imaging* **18** 538–48
- Paterson A, Frush D P and Donnelly L F 2001 Helical CT of the body: are settings adjusted for pediatric patients? *AJR Am. J. Roentgenol.* **176** 297–301
- Peitgen H-O, Jürgens H and Saupe D 1992 *Chaos and Fractals: New Frontiers of Science* (New York: Springer)
- Rangayyan R M, Dhawan A P and Gordon R 1985 Algorithms for limited-view computed tomography: an annotated bibliography and a challenge *App. Opt.* **24** 4000–12
- Ray T S and Jan N 1994 Anomalous approach to the self-organized critical state in a model for life at the edge of chaos *Phys. Rev. Lett.* **72** 4045–8
- Smith J M 1995 Life at the edge of chaos? *New York Review* (New York) pp 28–30
- Tam K C, Lauritsch G and Sourbelle K 2002 Filtering point spread function in backprojection cone-beam CT and its applications in long object imaging *Phys. Med. Biol.* **47** 2685–703
- Tanaka E 1987 A fast reconstruction algorithm for stationary positron emission tomography based on a modified EM algorithm *IEEE Trans. Med. Imaging* **6** 98–105
- Tang X and Ning R 2001 A cone beam filtered backprojection (CB-FBP) reconstruction algorithm for a circle-plus-two-arc orbit *Med. Phys.* **28** 1042–55
- Thomas J 2003 *Coupled Map Lattices* <http://chaos.phy.ohiou.edu/~thomas/index.html>
- Waldrop M M 1992 *Complexity: The Emerging Science at the Edge of Order and Chaos* (New York: Simon and Schuster)
- Wang G, Vannier M W and Cheng P C 1999 Iterative X-ray cone-beam tomography for metal artifact reduction and local region reconstruction *Microsc. Microanal.* **5** 58–65
- Weng Y, Zeng G L and Gullberg G T 1996 Filtered backprojection algorithms for attenuated parallel and cone-beam projections sampled on a sphere *Three-Dimensional Reconstruction in Radiology and Nuclear Medicine* ed P Grangeat and J-L Amans (Dordrecht: Kluwer) pp 19–34
- Wiest P W, Locken J A, Heintz P H and Mettler F A Jr 2002 CT scanning: a major source of radiation exposure *Semin. Ultrasound Ct Mr* **23** 402–10